Modelling lower-limb peripheral arterial disease using clinically available datasets: impact of inflow boundary conditions on hemodynamic indices for restenosis prediction

Federica Ninno[1,2], Claudio Chiastra[3], Monika Colombo[4], Alan Dardik[5,6], David Strosberg[6,7], Edouard Aboian[6], Janice Tsui[8,9], Matthew Bartlett[9,10], Stavroula Balabani[2,10] and Vanessa Díaz-Zuccarini[2,10*]

1. Department of Medical Physics and Biomedical Engineering, University College London, London, UK
2. Wellcome-EPSRC Centre for Interventional Surgical Sciences, London, UK
3. Polito[BIO]Med Lab, Department of Mechanical and Aerospace Engineering, Politecnico di Torino, Turin, Italy
4. Department of Mechanical and Production Engineering, Aarhus University, Aarhus, Denmark
5. Vascular Biology and Therapeutics, Yale University School of Medicine, New Haven, Connecticut, USA
6. Division of Vascular Surgery and Endovascular Therapy, Department of Surgery, Yale University School of Medicine, New Haven, Connecticut, USA
7. Department of Surgery, VA Connecticut Healthcare Systems, West Haven, Connecticut, USA
8. Department of Vascular Surgery, Royal Free Hospital NHS Foundation Trust, London, UK
9. Division of Surgery & Interventional Science, Department of Surgical Biotechnology, Faculty of Medical Sciences, University College London, London, UK
10. Department of Mechanical Engineering, University College London, London, UK

***Address for correspondence:**

Vanessa Díaz-Zuccarini, PhD

Department of Mechanical Engineering, University College London, London, UK

v.diaz@ucl.ac.uk

Abstract

Background and Objectives: The integration of hemodynamic markers as risk factors in restenosis prediction models for lower-limb peripheral arteries is hindered by fragmented clinical datasets. Computed tomography (CT) scans enable vessel geometry reconstruction and can be obtained at different times than the Doppler ultrasound (DUS) images, which provide information on blood flow velocity. Computational fluid dynamics (CFD) simulations allow the computation of near-wall hemodynamic indices, whose accuracy depends on the prescribed inlet boundary condition (BC), derived from the DUS images. This study aims to: (i) investigate the impact of different DUS-derived velocity waveforms on CFD results; (ii) test whether the same vessel areas, subjected to altered hemodynamics, can be detected independently of the applied inlet BC; (iii) suggest suitable DUS images to obtain reliable CFD results.

Methods: CFD simulations were conducted on three patients treated with bypass surgery, using patient-specific DUS-derived inlet BCs recorded at either the same or different time points than the CT scan. The impact of the chosen inflow condition on bypass hemodynamics was assessed in terms of wall shear stress (WSS)-derived quantities. Patient-specific critical thresholds for the hemodynamic indices were applied to identify critical luminal areas and compare the results with a reference obtained with a DUS image acquired in close temporal proximity to the CT scan.

Results: The main findings indicate that: (i) DUS-derived inlet velocity waveforms acquired at different time points than the CT scan led to statistically significantly different CFD results ($p<0.001$); (ii) the same luminal surface areas, exposed to low time-averaged WSS, could be identified independently of the applied inlet BCs; (iii) similar outcomes were observed for the other hemodynamic indices if the prescribed inlet velocity waveform had the same shape and comparable systolic acceleration time to the one recorded in close temporal proximity to the CT scan.

Conclusions: Despite a lack of standardised data collection for diseased lower-limb peripheral arteries, an accurate estimation of luminal areas subjected to altered near-wall hemodynamics is possible independently of the applied inlet BC. This holds if the applied inlet waveform shares some characteristics – derivable from the DUS report – as one matching the acquisition time of the CT scan.

Keywords

Peripheral arterial disease, Doppler ultrasound, Computational fluid dynamics**,** Uncertainty quantification, Inlet boundary conditions, Wall shear stress, Topological skeleton

1. Introduction

Lower-limb peripheral arterial disease (PAD) is a progressive pathology resulting in the obstruction of flow in the arterial system of the lower limbs, affecting over 200 million people worldwide[1]. The primary cause of lower-limb PAD is atherosclerosis, characterised by the buildup of lipid-rich plaque that gradually obstructs peripheral arteries. Surgical or endovascular treatments, like bypass or balloon-angioplasty with or without stent implantation, can be performed to restore blood flow and prevent severe consequences for the patient, such as limb amputation. However, despite initially achieving patency, these revascularisation procedures often lead to restenosis (i.e., the reoccurrence of vessel narrowing) due to different pathogenic mechanisms depending on the adopted treatment modality[2,3].

While it is fundamental to tailor surveillance and prevention programs for such a high prevalence clinical problem[4], determining when restenosis will occur for a specific patient is currently impossible, given the challenging and multifactorial nature of this adverse phenomenon. Numerous studies have addressed the issue of restenosis prediction, extending beyond PAD, and have identified not only routinely collected demographic, clinical, and angiographic risk factors but also altered hemodynamic indices linked to disease progression[5].

Revascularised vessel locations generally exhibit disturbed flow, caused by either balloon inflation and stent implantation or bypass procedures, and typically coincide with preferred sites for restenosis to progress[6]. Consequently, computing near-wall hemodynamic descriptors (i.e. wall shear stress (WSS)-related indices) and investigating their association with restenosis has been the subject of several studies in recent years[7–14]. This approach might allow the identification of vessel regions more

prone to developing restenosis and patients at higher risk. To date, the distribution of WSS and WSS-related indices in peripheral arteries cannot be estimated or measured except by performing computational fluid dynamics (CFD) simulations.

The reliability of the WSS-related indices is heavily dependent on patient-specific vessel geometry reconstruction and the conditions applied at the boundary of the fluid domain. These factors represent a source of uncertainty undermining the potential clinical applicability of the WSS-related indices and their use in restenosis prediction models. In this regard, a major concern is related to the prescribed inflow boundary conditions (BCs)[15–23]. This issue becomes even more challenging when dealing with datasets regarding lower-limb peripheral arteries, as data collection is not standardised. Despite standard surveillance follow-ups mandated by the current clinical pathway – in the UK and Europe generally at 1, 3, 6 and 12 months post-intervention[24,25] – available datasets can be fragmented. Computed tomography (CT) or magnetic resonance (MR) scans, from which vessel geometry can be reconstructed, are acquired only under specific clinical indications. Doppler ultrasound (DUS) images, providing information regarding blood flow velocity, are not always stored, with only the DUS examination report archived for decision-making by doctors. Moreover, healthcare system limitations, patients' comorbidities and compliance hinder homogenised data collection.

In this context, when CT or MR scans are accessible, the available DUS images often do not correspond to the acquisition time of the former, resulting in mismatched information for vessel geometry and blood flow velocity. This, in turn, further reduces the pool of usable clinical images for conducting CFD analyses.

The impact of different inflow BCs on hemodynamic indices has been investigated in other vascular regions[15–18], and parabolic and uniform inlet velocity profiles have been compared to assess the

impact on the femoral arteries' hemodynamics[26]. However, the impact of applying inlet velocity waveforms – acquired at different time points than the information regarding vessel geometry – on the computation of WSS-derived indices has yet to be evaluated for lower-limb peripheral arteries. Moreover, it has not been tested whether the same critical luminal regions of the vessel, more prone to restenosis, could be depicted independently of the applied inlet BCs, potentially expanding the pool of usable clinical data.

Herein, we compared the near-wall hemodynamic results obtained by applying velocity waveforms acquired at different time points than the CT scan to the scenario where no mismatching is present. The final aim is to assess the differences in the hemodynamic indices when mismatching pieces of information are available, test whether the same critical luminal regions for restenosis can be identified, and provide indications on which available DUS image could produce more reliable CFD results.

2. Methods

Figure 1 presents the workflow of the study. This involved (i) vessel three-dimensional (3D) reconstruction from CT scans, followed by (ii) the configuration of patient-specific CFD simulations, where the inlet BC was defined by applying the DUS-derived velocity waveforms acquired at the same and different time points than the CT scans, and (iii) post-processing of the results. Every step is detailed in the subsections below.

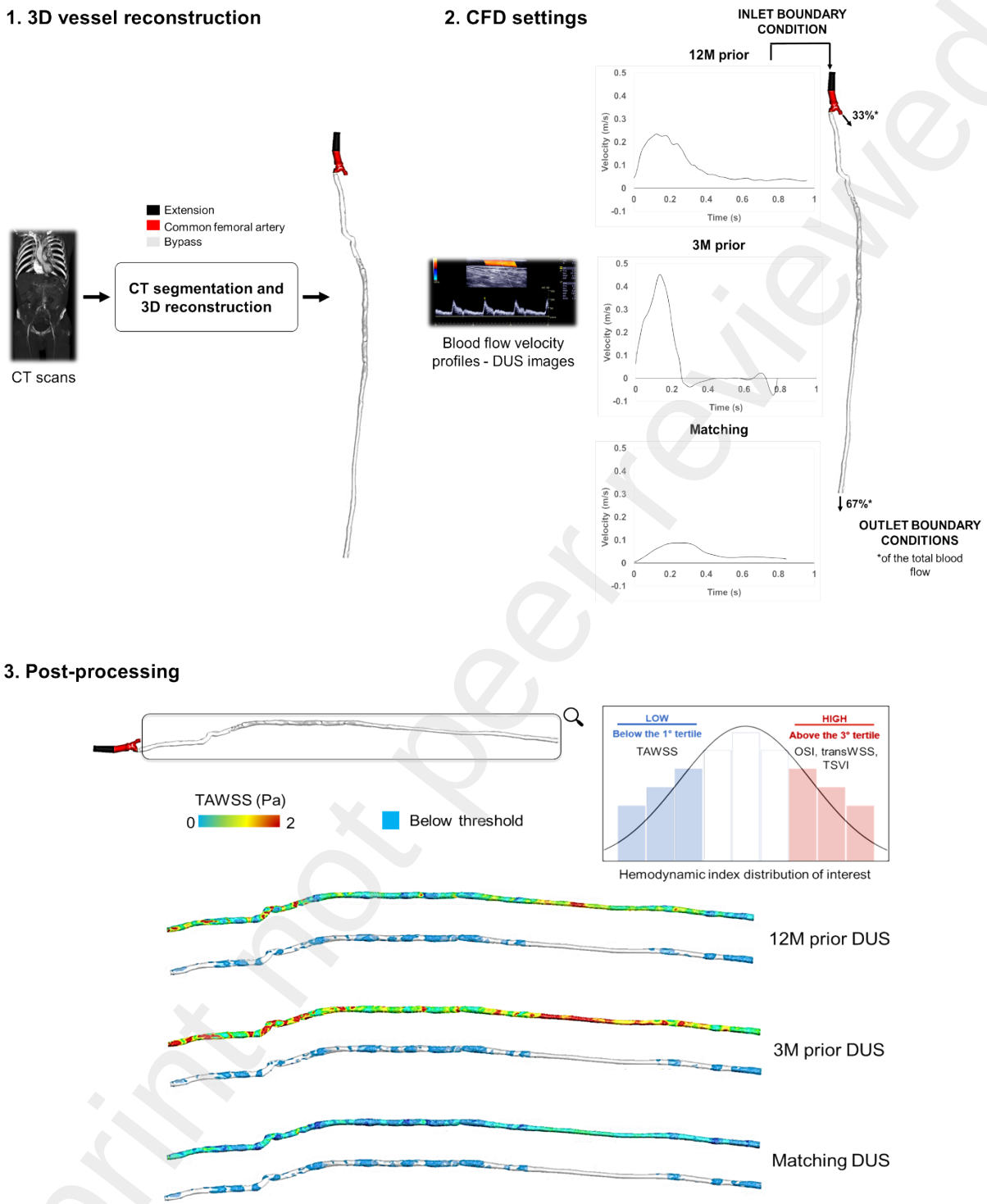

Figure 1. Workflow of the study. CT scans were used to reconstruct 3D models of the femoral arteries. DUS images acquired at the same time point ("Matching") and different ones (3-months (3M) and 12-months (12M) prior in this example) than the

CT scan were used as inlet boundary conditions. A literature-derived flow split[27] was applied at the outlets of the domain. The results were post-processed regarding WSS-derived indices of interest (time-averaged wall shear stress (TAWSS) in Figure) for every applied BC. Critical thresholds for the hemodynamic indices were identified based on their distributions. Critical regions on the bypass (below threshold in this example for TAWSS) were highlighted.

2.1 Patient dataset and 3D vessel reconstruction

Three patients suffering from PAD who underwent femoropopliteal bypass surgery (autologous vein graft) and had one available CT scan and different stored DUS, one matching the acquisition time point of the geometry information, were considered in the study. Table 1 summarises the clinical dataset, including revascularised limb, bypass length and acquisition dates of CT scans and DUS images. There was no registered change in the clinical status, and no intervention was performed between the acquisition of the CT scans and the DUS images matching the acquisition time point of the former. When acquired close enough to the CT scan data, the DUS images are referred to as "Matching", whereas "prior" and "follow-up (FU)" terms pertain to acquisitions that happened some months (M) before or after the CT scan, respectively. The deidentified data were received from VA Connecticut Healthcare Systems (West Haven, CT, USA). The study was ethically approved by West Haven VA Connecticut Healthcare Systems (approval number AD0009).

Each femoropopliteal artery was segmented and 3D reconstructed using a previously validated semi-automatic algorithm[26] implemented in MATLAB (MathWorks, Natick, MA, USA). The bypass reconstruction was carried out until just before reaching bypass distal anastomosis, due to poor contrast agent in that specific region.

Table 1. Clinical dataset adopted in the present study. The DUS images were acquired at the same time point (Matching) or several months (M) prior/following-up (FU) the CT scan acquisition.

Dataset	Revascularised limb	Bypass length (mm)	CT scan acquisition (dd/mm/yyyy)	DUS acquisition (dd/mm/yyyy)
Patient 1 (PT1)	Left	623	18/10/2022	Matching – 25/10/2022 12M prior – 03/11/2021 3M prior – 22/07/2022
Patient 2 (PT2)	Left	574	28/06/2020	Matching – 27/06/2020 26M prior – 18/05/2018 5M FU – 18/11/2020 11M FU – 26/05/2021
Patient 3 (PT3)	Right	595	19/02/2022	Matching – 21/02/2022 12M prior – 10/02/2021 6M prior – 26/08/2021 2M FU – 20/04/2022

2.2 Computational fluid dynamics simulations

As a first step to configure the patient-specific CFD simulations, the fluid domain was discretised using the software ICEM CFD (Ansys Inc., Canonsburg, PA, USA), combining tetrahedral elements with 5 layers of prismatic elements close to the wall. The adopted meshing parameters were defined following a previous mesh independence study[26]. The discretised Navier-Stokes and continuity equations were solved in Fluent (Ansys Inc.). The flow was assumed as laminar[26], and blood density was considered

constant and equal to 1060 kg/m^3. Blood's non-Newtonian behaviour was modelled using the Carreau model[26].

For each 3D reconstructed femoropopliteal bypass, transient CFD simulations were conducted, each testing the inlet velocity waveforms extracted from the available DUS images. The blood velocity waveforms were all acquired at the common femoral artery level, coinciding with the inlet boundary of the geometry domain. The waveforms were manually extracted from the DUS spectrum, and the sequence of peak velocities was elaborated in MATLAB by applying the algorithm of Ponzini et al.[28], as detailed in Colombo et al.[26]. A Womersley velocity profile was imposed at the inlet cross-section. A literature-derived flow split was prescribed at the profunda femoral and bypass outlets – 33% and 67%, respectively[27]. The vessel wall was assumed to be rigid with no-slip conditions. A pressure-based solver with a coupled scheme for the pressure-velocity coupling was employed, utilising second-order, second-order upwind and least-squares cell-based schemes for pressure, momentum and gradient spatial discretisation, respectively[26]. The under-relaxation factors for pressure and momentum were set to 1. The Fluent flow Courant number was set to 50, and explicit relaxation factors for momentum and pressure were set to 0.3[26]. A convergence criterion of 5×10^{-5} was chosen for continuity and velocity residuals based on a sensitivity analysis[26]. The simulation of two cardiac cycles proved sufficient to guarantee repeatable solutions[26]. An additional sensitivity analysis established the best temporal discretisation (100 time steps per cardiac cycle) for reliability and computational cost-effectiveness[26].

2.3 Near-wall hemodynamic indices

The impact of the adopted DUS-derived velocity waveform on the CFD results was assessed by analysing the near-wall hemodynamics of the bypass region of each case.

Specifically, WSS-based descriptors accounting for the magnitude (time-averaged WSS, TAWSS), oscillatory (oscillatory shear index, OSI) and multidirectional nature (transverse WSS, transWSS)[8,9,29–33] of the WSS field over the cardiac cycle were computed along the bypass luminal wall (Figure 2).

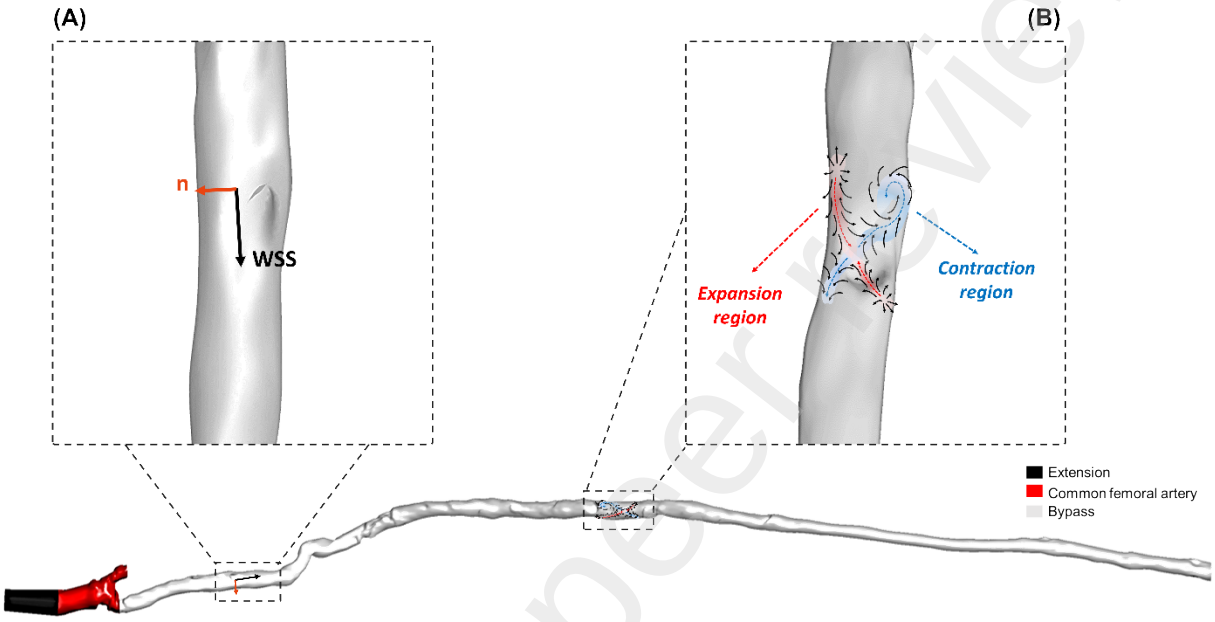

WSS-based descriptors

Time-averaged WSS (TAWSS)	Cardiac cycle-averaged WSS vector (black arrow) magnitude	$\mathrm{TAWSS} = \frac{1}{\mathrm{T}}\int_0^{\mathrm{T}} \lvert\mathbf{WSS}\rvert \, \mathrm{dt}$
Oscillatory Shear Index (OSI)	A measure the directional change of WSS during the cardiac cycle, accounting for the degree of flow reversal. It ranges between 0 (totally unidirectional WSS vector) and 0.5 (purely oscillatory WSS with a net magnitude of zero)	$\mathrm{OSI} = 0.5\left[1 - \left(\frac{\left\lvert\int_0^{\mathrm{T}} \mathbf{WSS}\,\mathrm{dt}\right\rvert}{\int_0^{\mathrm{T}} \lvert\mathbf{WSS}\rvert \, \mathrm{dt}}\right)\right]$
Transverse WSS (TransWSS)	Average of the WSS vector component acting orthogonal to the cardiac cycle-averaged WSS vector direction	$\mathrm{transWSS} = \frac{1}{\mathrm{T}}\int_0^{\mathrm{T}} \left\lvert \mathbf{WSS} \cdot \left(\mathbf{n} \times \frac{\int_0^{\mathrm{T}} \mathbf{WSS}\,\mathrm{dt}}{\left\lvert\int_0^{\mathrm{T}} \mathbf{WSS}\,\mathrm{dt}\right\rvert} \right) \right\rvert \mathrm{dt}$
Topological Shear Variation Index (TSVI)	The root mean square deviation of the divergence of the normalized WSS vector with respect to its average over the cardiac cycle. It quantifies the variability of WSS contraction/expansion action exerted at the endothelium along the cardiac cycle (blue/red regions)	$\mathrm{TSVI} = \left\{\frac{1}{\mathrm{T}}\int_0^{\mathrm{T}} \left[\nabla\cdot(\mathbf{WSS}_{\mathrm{u}}) - \overline{\nabla\cdot(\mathbf{WSS}_{\mathrm{u}})}\right]^2 \mathrm{dt}\right\}^{1/2}$

Figure 2. Hemodynamic indices investigated in the present study. Figure adapted with permission from Candreva et al.[34]. T represents the cardiac cycle period over which values of the **WSS** vector are estimated. $\mathbf{WSS}_{\mathrm{u}}$ is the **WSS** vector normalised

by its magnitude. (A) Example of **WSS** vector acting on a generic point at the luminal surface (black arrow), with the unit vector **n** normal to the vessel wall (red arrow). (B) Explanatory maps of the **WSS** vector field (black arrows) with the identified contraction/expansion regions (in blue and red, respectively) at the luminal surface.

Regions on the lumen subjected to low values of TAWSS (below 0.5 Pa[35–37]) are highly likely to be preferred sites for restenosis[6,8,9,33] due to a stimulated proatherogenic endothelial phenotype. Luminal areas subjected to higher OSI values than 0.2[38] might coincide with disturbed flow and the development of pathogenic mechanisms[8,9,33], and high values of transWSS can co-locate with regions more prone to wall remodelling[8,9,31–33].

Additionally, an analysis of the WSS topological skeleton was conducted through an Eulerian-based method relying on the divergence of the WSS vector field[39]. Namely, the Topological Shear Variation Index (TSVI) (Figure 2) was used to evaluate the variability of the local contraction/expansion action exerted by the WSS on the bypass lumen along the cardiac cycle[34,40]. Recent findings showed that high values of TSVI are potentially linked with vascular dysfunction and with areas more susceptible to remodelling[41–45].

2.4 Statistical analysis, critical regions identification and co-localisation

The Shapiro-Wilk test was employed to verify the normality of the hemodynamic indices' distribution for each applied inlet BC. Pairwise comparisons between the reference distribution of each hemodynamic index (i.e., when no temporal mismatch is present) and those obtained when other velocity waveforms are applied at the inlet, were performed using the non-parametric Wilcoxon test to assess significant differences. All statistical analyses were conducted using MATLAB, and statistical significance was assumed for p-values < 0.05.

Thresholds for critical values (high or low) of the hemodynamic indices were computed for each hemodynamic index distribution and applied BC. This involved quantifying the 33rd percentile (low values) or the 66th percentile (high values) of the distribution, considering luminal regions as critical if they exhibited values lower or higher than the threshold[8].

The co-localisation of the identified low/high hemodynamic values on the luminal wall obtained with different inlet BCs to the reference results was assessed by applying the Jaccard similarity index (SI)[15,46]:

$$SI = \frac{2(Indexperc_{Match} \cap Indexperc_{BC})}{(Indexperc_{Match} \cup Indexperc_{BC})}$$

where $Indexperc_{Match}$ is the luminal surface area exposed to low (33rd percentile) or high (66th percentile) values when a "Matching" DUS is applied as inlet BC and $Indexperc_{BC}$ is the luminal surface area exposed to either low or high values when other available DUS images are used. The SI ranges from 0 (no co-localisation) to 1 (perfect co-localisation). This metric determined whether the same critical regions observed when applying a "Matching" DUS as inlet BC could be depicted independently of the applied DUS.

3. Results

3.1 DUS-derived velocity waveforms

Figure 3 shows the extracted patient-specific velocity waveforms for PT1, PT2 and PT3. Table 2 summarises the waveform shape, peak systolic velocity, systolic acceleration time and cardiac cycle period of the available DUS for every patient.

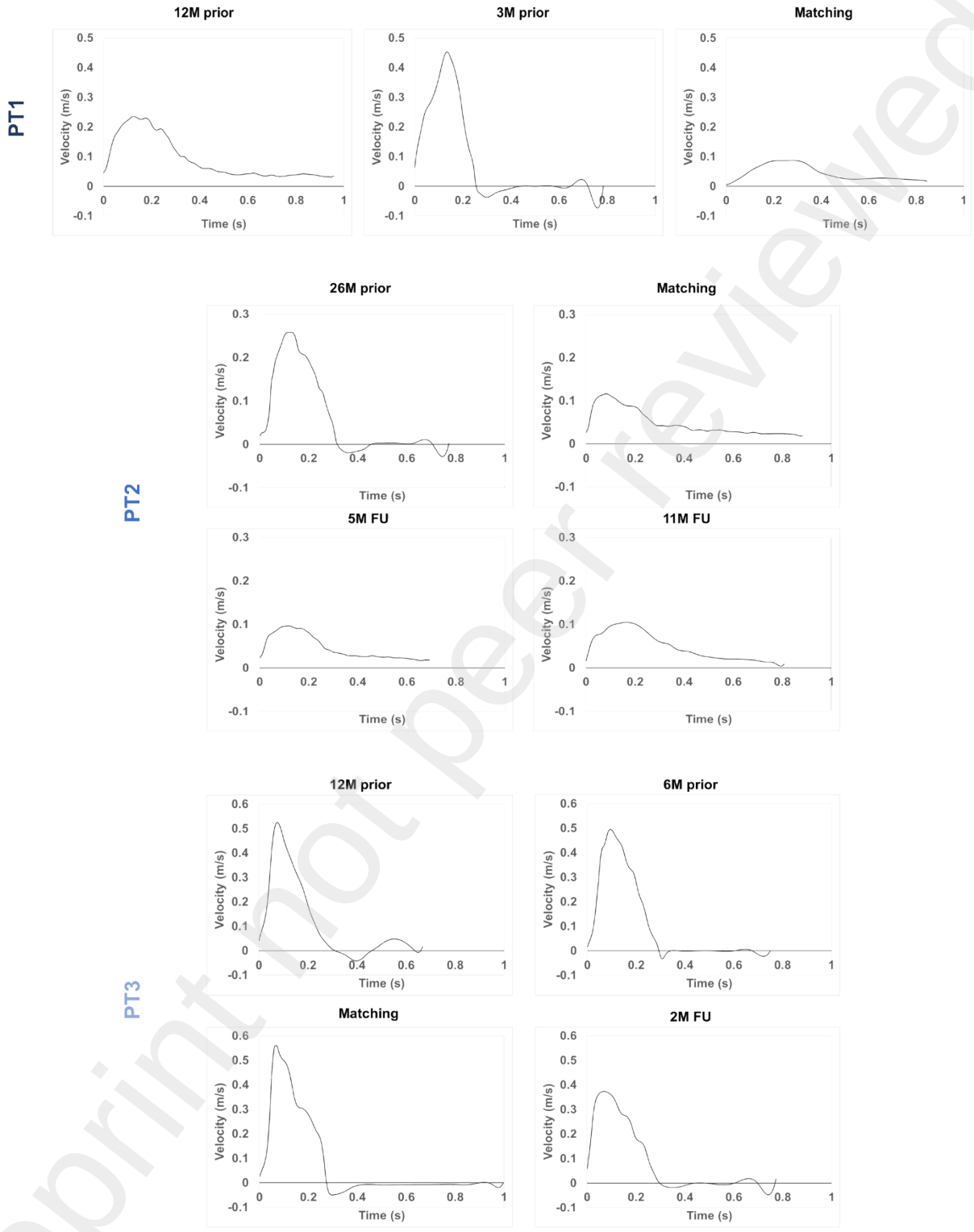

Figure 3. Extracted patient-specific velocity waveforms for every patient and time point.

Table 2. DUS-derived waveforms' characteristics for every patient and time point regarding waveform shape, peak systolic velocity, systolic acceleration time and cardiac cycle period.

PT1	**Waveform shape**	**Peak systolic velocity (m/s)**	**Systolic acceleration time (s)**	**Cardiac cycle period (s)**
12M prior	Monophasic	0.235	0.126	0.968
3M prior	Biphasic	0.453	0.135	0.792
Matching	Monophasic	0.087	0.273	0.854
PT2	**Waveform shape**	**Peak systolic velocity (m/s)**	**Systolic acceleration time (s)**	**Cardiac cycle period (s)**
26M prior	Biphasic	0.257	0.125	0.780
Matching	Monophasic	0.116	0.080	0.892
5M FU	Monophasic	0.097	0.119	0.700
11M FU	Monophasic	0.105	0.163	0.816
PT3	**Waveform shape**	**Peak systolic velocity (m/s)**	**Systolic acceleration time (s)**	**Cardiac cycle period (s)**
12M prior	Triphasic	0.525	0.074	0.674
6M prior	Biphasic	0.494	0.091	0.757
Matching	Biphasic	0.560	0.070	1.007
2M FU	Biphasic	0.374	0.070	0.781

For PT1, Matching and 12M prior velocity waveforms were monophasic, meaning that the waveforms did not cross the zero-flow baseline at any part of the cardiac cycle, and blood flowed in the antegrade direction[47]. 12M prior peak systolic velocity and systolic acceleration time were more than double and halved with respect to the matching ones, respectively (Table 2). The 3M prior velocity waveform was biphasic, presenting retrograde flow in the early diastolic phase but lacking a third phase potentially due to distal compliance loss.

For PT2, monophasic waveforms were recorded at Matching and all follow-up time points, with peak systolic velocity and systolic acceleration time almost comparable for the Matching (0.116 m/s, 0.080 s) and the 5M follow-up (0.097 m/s, 0.119 s). However, the two waveforms exhibited different periods (0.892 s and 0.700 s, respectively). A biphasic waveform was depicted for the DUS acquired 26M prior to the CT scan.

For PT3, the Matching, 6M prior and 2M FU DUS-derived velocity waveforms were biphasic, whereas the 12M was triphasic. The 12M, Matching, and 2M FU waveforms had comparable systolic acceleration time (around 0.070 s), although the latter had a lower peak systolic velocity (0.374 m/s) compared to the former ones (0.525 m/s and 0.560 m/s, respectively).

3.2 Impact of mismatching DUS-derived waveforms on the hemodynamic indices

Figure 4 depicts the hemodynamic index distributions obtained for each patient and applied BC.

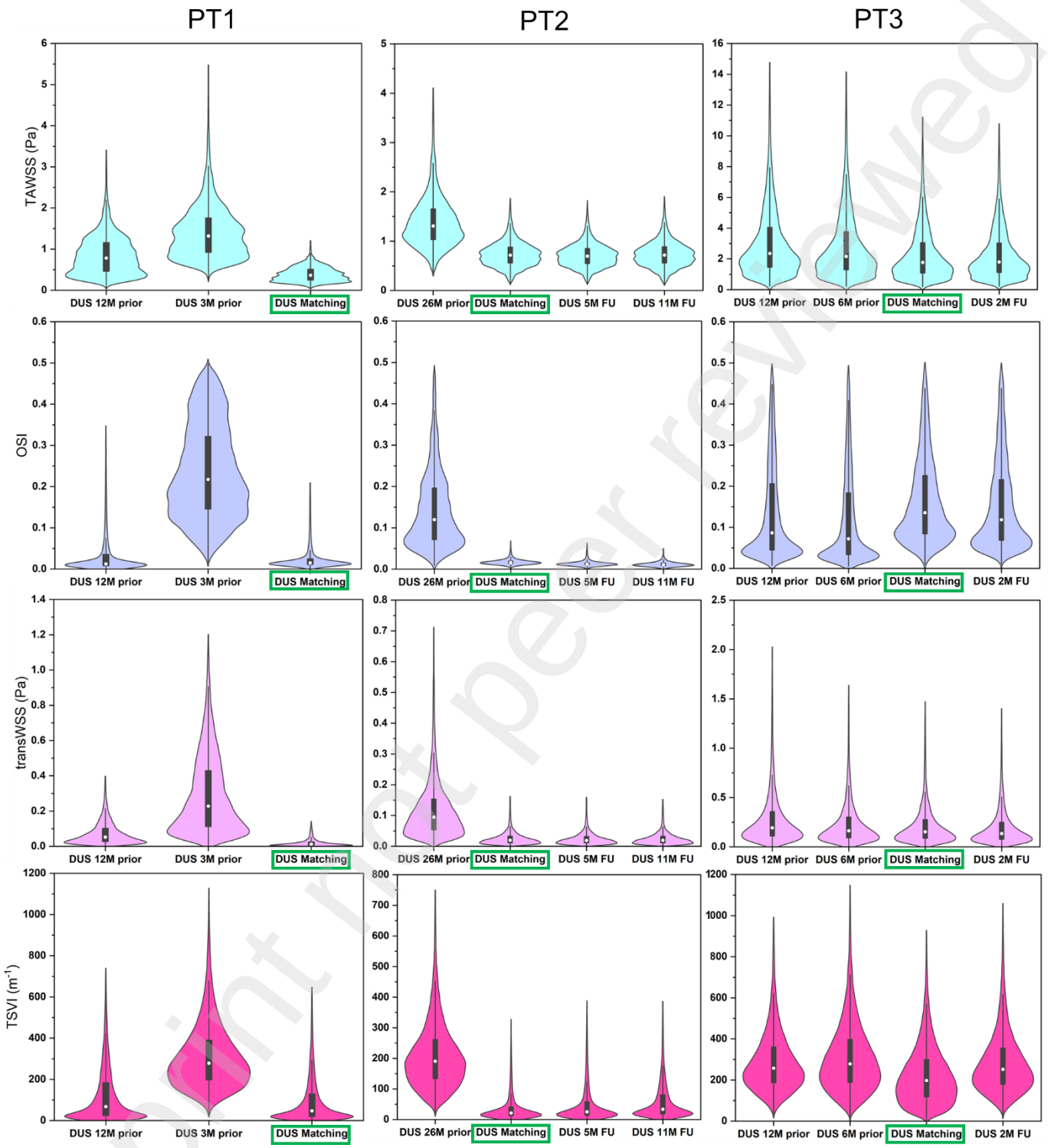

Figure 4. TAWSS, OSI, transWSS and TSVI distributions for every patient and applied BC. The reference distributions – obtained when applying a "Matching" DUS – are highlighted by a rectangle.

Table 1 in Supplementary Material summarises the median values for every distribution. Almost all distributions of WSS-derived indices were strongly statistically significantly different ($p < 0.001$, Table 1 in Supplementary Material) from the one obtained when the acquisition of the DUS matched the acquisition time point of the CT scan. One exception was represented by the TAWSS distribution of PT2 when applying the recorded 11M prior DUS waveform ($p = 0.23$). Although some median values of the hemodynamic indices' distributions were comparable with the reference results, the non-parametric test indicated that statistically significantly different results for TAWSS, OSI, transWSS and TSVI would be obtained in case of missing DUS acquired at the same time point as the CT scan.

3.3 Identification of critical areas and co-localisation with reference results

The computation of the hemodynamic indices' distribution for each patient and BC allowed the identification of the patient-specific critical thresholds, as reported in Table 2 in Supplementary Material.

Regarding the TAWSS and OSI indices, some patient-specific thresholds were comparable with the critical values reported in the literature, below and above which a link with disease progression has been demonstrated[35–38]. Nevertheless, for some waveforms, the critical value for the OSI index was around 10 times lower than the one reported in the literature[38] (PT1 with 12M prior and Matching DUS; PT2 with Matching, 5MFU and 11M FU DUS), raising concerns about computing patient-specific critical thresholds to avoid losing any information when trying to identify potentially critical areas for restenosis. No comparisons with literature could be performed for the transWSS and TSVI distribution thresholds, due to lack of reported absolute critical values. Figure 5 illustrates the identified critical luminal areas on the bypass region for PT1 for each applied BC. The corresponding results for PT2 and PT3 are presented in Supplementary Material (Figures 1 and 2, respectively).

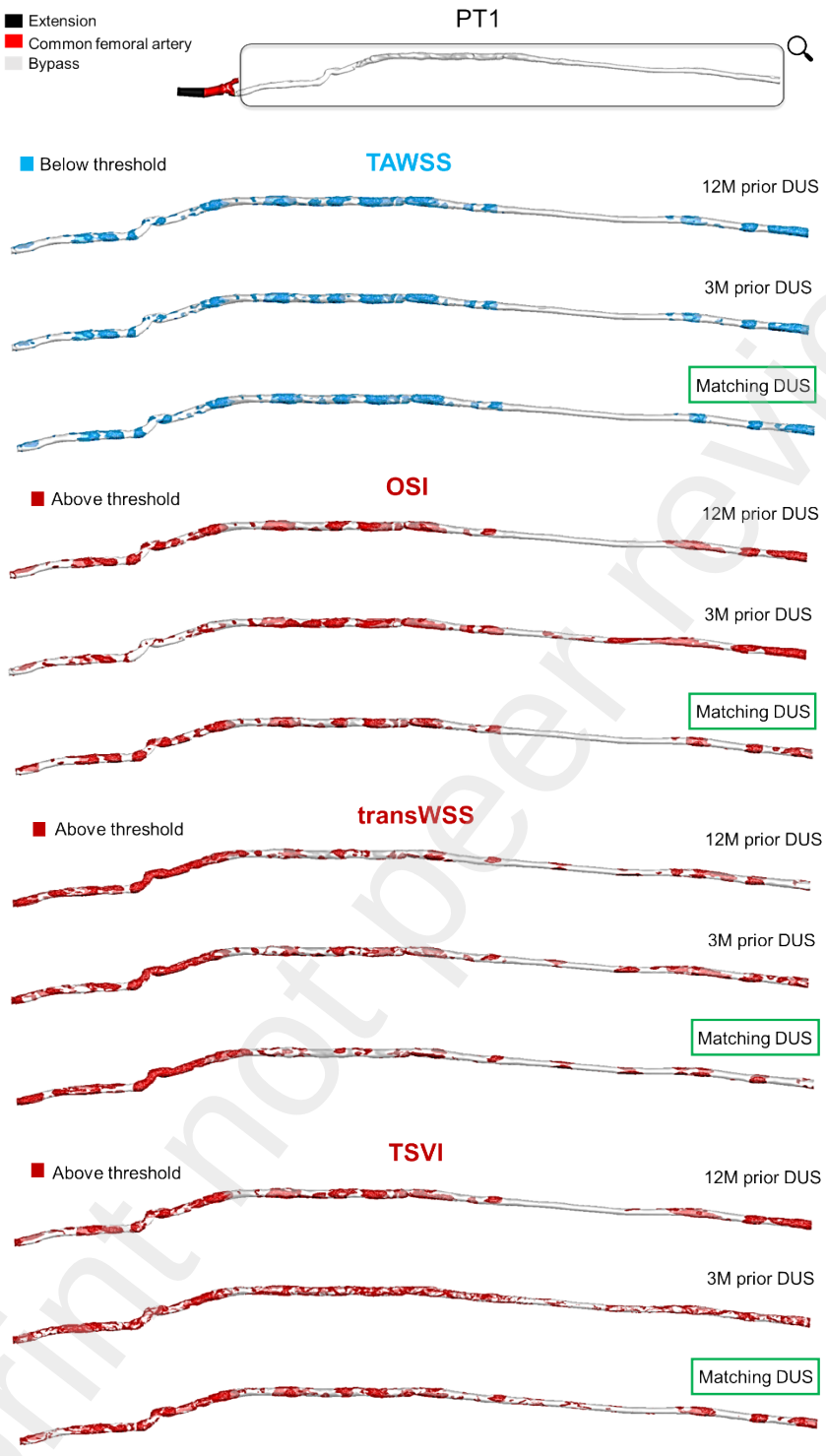

Figure 5. Identified critical areas – more prone to restenosis – above/below patient-specific thresholds for PT1. The reference critical regions – obtained when applying a "Matching" DUS – are highlighted by a rectangle.

The similarity indices for each patient and applied DUS-derived waveforms are summarised in Table 3.

Table 3. Similarity indices to reference results ("Matching" DUS) in terms of identified critical luminal areas for PT1, PT2 and PT3 for each hemodynamic index and BC.

Similarity Index (PT1)	**12M prior - Matching**	**3M prior - Matching**	
TAWSS	0.87	0.84	
OSI	0.82	0.54	
transWSS	0.78	0.61	
TSVI	0.72	0.49	
Similarity Index (PT2)	**26M prior - Matching**	**5M FU - Matching**	**11M FU - Matching**
TAWSS	0.90	0.98	0.99
OSI	0.66	0.96	0.95
transWSS	0.72	0.97	0.95
TSVI	0.55	0.88	0.65
Similarity Index (PT3)	**12M prior - Matching**	**6M prior - Matching**	**2M FU - Matching**
TAWSS	0.97	0.96	0.96
OSI	0.81	0.83	0.87
transWSS	0.87	0.85	0.86
TSVI	0.64	0.58	0.63

It is noteworthy that the similarity indices for the TAWSS were remarkably high (range: 0.84-0.99) for every patient and applied BC. Moreover, the similarity indices for the OSI remained high when the shape of the applied waveform was the same as the "Matching" one (monophasic: PT1 with 12M prior DUS; PT2 with 5M and 11M FU DUS; biphasic: PT3 with 6M prior and 2M FU DUS). The similarity index substantially dropped when the velocity waveform was remarkably different from the "Matching" one (PT1 with 3M prior DUS, PT2 with 26M prior DUS). Similar behaviour as the OSI was observed for the transWSS index, although the drop in the similarity index was not as dramatic as the one for the OSI. Finally, the similarity index for the TSVI remarkably dropped for every patient and applied BC. However, higher values were reported in the case of the same shape and closer systolic acceleration time to the Matching DUS, independently from the peak systolic velocity and cardiac cycle period (SI:0.72 for PT1 with 12M DUS; SI: 0.88 for PT2 with 5M FU DUS; SI:0.63 for PT3 with 2M FU DUS).

4. Discussion

The present study involved a comparative analysis of the CFD results obtained in three diseased lower-limb femoropopliteal arteries. The inlet blood flow velocity waveforms were derived from DUS images acquired at the same and different time points than the CT scan, from which vessel geometry was reconstructed. The analysis compared the obtained hemodynamic indices' distributions, identified the vessel regions exposed to altered hemodynamic indices, and assessed the co-localisation of the identified critical luminal areas with the ideal case of the CT scan and DUS images acquired at the same point in time.

The rationale of this work lies in the extensive research on uncertainty quantification in patient-specific vascular models. The key to the translation of hemodynamic indices into clinical biomarkers for vascular disease prediction relies on a more nuanced understanding of the impact of modelling assumptions, with particular emphasis on the primary role played by the prescribed inlet conditions. Extending beyond PAD, this has been the subject of studies in the context of modelling coronary[15,16] and aortic[18–23] flows, all firmly corroborating the influence of different inlet conditions on the near-wall hemodynamic indices.

The main findings of the study can be summarised as follows: (i) a DUS-derived inlet velocity waveform that is not representative of the actual hemodynamic condition (i.e., acquired before or after the CT scan) might produce statistically significantly different hemodynamic results to the ones obtained when the DUS image acquisition matches in time the CT scan; (ii) patient-specific critical thresholds obtained from the hemodynamic indices' distributions allow accurate identification of the same critical luminal regions, independently from the applied inlet BC; (iii) for the TAWSS index, the accuracy of the co-localisation of the critical areas with respect to the ideal case is above 84% for every considered patient and applied BC. Firstly, this result confirms what was found in the coronary arteries, where luminal surface areas exposed to low WSS showed robustness to the applied flow rate values obtained from four different in vivo assessment techniques[15]. Secondly, this finding is encouraging because luminal areas exposed to low TAWSS were found to be positively correlated with lumen area change in stented superficial femoral arteries[8,9], and it might be particularly crucial to accurately depict these critical areas when predicting restenosis development; (iv) for the OSI, transWSS and TSVI indices, this accuracy drops but it can be partially compensated if the applied inlet velocity waveform has the same shape and comparable systolic acceleration time as the one matching in time the CT scan acquisition. In

addition, the results indicate that the major contribution is given by the shape of the waveform, followed by the systolic acceleration time and all other waveform characteristics, such as peak systolic velocity and the period of the cardiac cycle. However, for the TSVI index, the accuracy of the co-localisation will always be lower than for the other indices. This metric depends not only on the magnitude of the WSS vector applied to a point on the vessel wall along the cardiac cycle, whose distribution shifts depending on the applied waveform velocity, but on the instantaneous WSS vector field configuration in a neighbourhood of such a point[41,43].

Several considerations have to be taken into account while interpreting the findings of this study. DUS accuracy depends on the intrinsic properties of the ultrasound beam, and the measurements also suffer from operator dependence. However, this source of error is challenging to minimise, and it is reasonable to expect that this does not compromise the overall discussion of the study. The prescribed outflow conditions are derived from literature and are not patient-specific. Moreover, the flow-split values are based on healthy vessels[27]. While using patient-specific flow-split values could enhance accuracy, deriving these values from DUS measurements introduces uncertainties. Nonetheless, a different flow rate through the modelled branches might not substantially impact the generalizability of the findings. Lastly, the absence of follow-up computed tomography (CT) scans prevents an assessment of whether the identified critical areas on the vessel wall, more prone to restenosis, actually underwent re-occlusion. However, it is important to note that this goes beyond the scope of the study, which regards the feasibility of obtaining reliable CFD results with fragmented datasets for patients with PAD.

5. Conclusions

In this study, DUS-derived velocity waveforms recorded at the same time or before/after the imaging data for vessel reconstruction (CT scan) were tested as inlet boundary conditions. The results reveal that, when the DUS is not acquired close enough in time to the CT scan, misleading conclusions can be drawn regarding the computed hemodynamic indices linked to restenosis development. However, such differences are not significant in terms of luminal surface areas exposed to low TAWSS and can be minimised for areas exposed to high OSI, transWSS and TSVI, if any available DUS waveform presents the same shape and comparable systolic acceleration time than the one observed when the CT scan was acquired. This information can be retrieved from the report on the DUS examination, which is always performed. This suggests that luminal areas subjected to altered hemodynamics can be potentially used to inform restenosis prediction models. Although the dataset is fragmented, these areas can be estimated well, enlarging the readily available clinical data that can be used to identify high-risk patients for restenosis.

Declarations

Funding

This work was supported by University College London EPSRC Centre for Doctoral Training i4health [EP/S021930/1] and the Wellcome/EPSRC Centre for Interventional and Surgical Sciences (WEISS) [203145Z/16/Z] fundings, by EPSRC Research Grant "Hidden haemodynamics: A Physics-InfOrmed, real-time recoNstruction framEwork for haEmodynamic virtual pRototyping and clinical support (PIONEER)" [EP/W00481X/1] and the resources and the use of facilities at the VA Connecticut Healthcare System, West Haven, CT, USA.

Competing interests

The authors declare that they have no competing interests.

References

1. Fowkes, F. G. R. *et al.* Peripheral artery disease: Epidemiology and global perspectives. *Nature Reviews Cardiology* vol. 14 Preprint at https://doi.org/10.1038/nrcardio.2016.179 (2017).

2. Schillinger, M. *et al.* Balloon angioplasty and stent implantation induce a vascular inflammatory reaction. *Journal of Endovascular Therapy* **9**, (2002).

3. Jukema, J. W., Verschuren, J. J. W., Ahmed, T. A. N. & Quax, P. H. A. Restenosis after PCI. Part 1: Pathophysiology and risk factors. *Nature Reviews Cardiology* vol. 9 Preprint at https://doi.org/10.1038/nrcardio.2011.132 (2012).

4. Sherif, M. Angioplasty and stenting for peripheral arterial disease of the lower limbs. *E-Journal of Cardiology Practice* Preprint at (2018).

5. Ninno, F., Tsui, J., Balabani, S. & Diaz-Zuccarini, V. A systematic review of clinical and biomechanical engineering perspectives on the prediction of restenosis in coronary and peripheral arteries. *JVS Vasc Sci* (2023) doi:10.1016/j.jvssci.2023.100128.

6. VanderLaan, P. A., Reardon, C. A. & Getz, G. S. Site Specificity of Atherosclerosis: Site-Selective Responses to Atherosclerotic Modulators. *Arteriosclerosis, Thrombosis, and Vascular Biology* vol. 24 Preprint at https://doi.org/10.1161/01.ATV.0000105054.43931.f0 (2004).

7. Gökgöl, C., Diehm, N., Räber, L. & Büchler, P. Prediction of restenosis based on hemodynamical markers in revascularized femoro-popliteal arteries during leg flexion. *Biomech Model Mechanobiol* (2019) doi:10.1007/s10237-019-01183-9.

8. Colombo, M. *et al.* Baseline local hemodynamics as predictor of lumen remodeling at 1-year follow-up in stented superficial femoral arteries. *Sci Rep* **11**, (2021).

9. Colombo, M. *et al.* In-Stent Restenosis Progression in Human Superficial Femoral Arteries: Dynamics of Lumen Remodeling and Impact of Local Hemodynamics. *Ann Biomed Eng* **49**, (2021).

10. Donadoni, F., Pichardo-Almarza, C., Homer-Vanniasinkam, S., Dardik, A. & Díaz-Zuccarini, V. Multiscale, patient-specific computational fluid dynamics models predict formation of neointimal hyperplasia in saphenous vein grafts. *J Vasc Surg Cases Innov Tech* **6**, (2020).

11. Conti, M. *et al.* Patient-specific computational fluid dynamics of femoro-popliteal stent-graft thrombosis. *Med Eng Phys* **86**, (2020).

12. Ferrarini, A. *et al.* Impact of leg bending in the patient-specific computational fluid dynamics of popliteal stenting. *Acta Mechanica Sinica/Lixue Xuebao* **37**, (2021).

13. Gökgöl, C., Diehm, N., Nezami, F. R. & Büchler, P. Nitinol Stent Oversizing in Patients Undergoing Popliteal Artery Revascularization: A Finite Element Study. *Ann Biomed Eng* (2015) doi:10.1007/s10439-015-1358-8.

14. Gökgöl, C. *et al.* Towards a better understanding of the posttreatment hemodynamic behaviors in femoropopliteal arteries through personalized computational models based on OCT images. *Sci Rep* **11**, (2021).

15. Lodi Rizzini, M. *et al.* Modelling coronary flows: impact of differently measured inflow boundary conditions on vessel-specific computational hemodynamic profiles. *Comput Methods Programs Biomed* **221**, (2022).

16. Lodi Rizzini, M. *et al.* Does the inflow velocity profile influence physiologically relevant flow patterns in computational hemodynamic models of left anterior descending coronary artery? *Med Eng Phys* **82**, (2020).

17. Pereira, V. M. *et al.* Evaluation of the influence of inlet boundary conditions on computational fluid dynamics for intracranial aneurysms: A virtual experiment. *J Biomech* **46**, (2013).

18. Stokes, C. *et al.* Aneurysmal growth in type-B aortic dissection: assessing the impact of patient-specific inlet conditions on key haemodynamic indices. *J R Soc Interface* **20**, (2023).

19. Armour, C. H. *et al.* The influence of inlet velocity profile on predicted flow in type B aortic dissection. *Biomech Model Mechanobiol* **20**, (2021).

20. Morbiducci, U., Ponzini, R., Gallo, D., Bignardi, C. & Rizzo, G. Inflow boundary conditions for image-based computational hemodynamics: Impact of idealized versus measured velocity profiles in the human aorta. *J Biomech* (2013) doi:10.1016/j.jbiomech.2012.10.012.

21. Pirola, S. *et al.* Computational study of aortic hemodynamics for patients with an abnormal aortic valve: The importance of secondary flow at the ascending aorta inlet. *APL Bioeng* **2**, (2018).

22. Madhavan, S. & Kemmerling, E. M. C. The effect of inlet and outlet boundary conditions in image-based CFD modeling of aortic flow. *Biomed Eng Online* **17**, (2018).

23. Youssefi, P. *et al.* Impact of patient-specific inflow velocity profile on hemodynamics of the thoracic aorta. *J Biomech Eng* **140**, (2018).

24. Neumann, F. J. *et al.* 2018 ESC/EACTS Guidelines on myocardial revascularization. *European Heart Journal* vol. 40 Preprint at https://doi.org/10.1093/eurheartj/ehy394 (2019).

25. Aboyans, V. *et al.* 2017 ESC Guidelines on the Diagnosis and Treatment of Peripheral Arterial Diseases, in collaboration with the European Society for Vascular Surgery (ESVS). *European Heart Journal* vol. 39 Preprint at https://doi.org/10.1093/eurheartj/ehx095 (2018).

26. Colombo, M. *et al.* Computing patient-specific hemodynamics in stented femoral artery models obtained from computed tomography using a validated 3D reconstruction method. *Med Eng Phys* (2020) doi:10.1016/j.medengphy.2019.10.005.

27. Klein, W. M., Bartels, L. W., Bax, L., Van der Graaf, Y. & Mali, W. P. T. M. Magnetic resonance imaging measurement of blood volume flow in peripheral arteries in healthy subjects. *J Vasc Surg* (2003) doi:10.1016/S0741-5214(03)00706-7.

28. Ponzini, R., Vergara, C., Redaelli, A. & Veneziani, A. Reliable CFD-based estimation of flow rate in haemodynamics measures. *Ultrasound Med Biol* (2006) doi:10.1016/j.ultrasmedbio.2006.05.022.

29. Mohamied, Y., Sherwin, S. J. & Weinberg, P. D. Understanding the fluid mechanics behind transverse wall shear stress. *J Biomech* **50**, (2017).

30. Poulsen, C. B. *et al.* Inducing persistent flow disturbances accelerates atherogenesis and promotes thin cap fibroatheroma development in D374Y-PCSK9 hypercholesterolemic minipigs. *Circulation* **132**, (2015).

31. Ene-Iordache, B., Semperboni, C., Dubini, G. & Remuzzi, A. Disturbed flow in a patient-specific arteriovenous fistula for hemodialysis: Multidirectional and reciprocating near-wall flow patterns. *J Biomech* **48**, (2015).

32. Bozzetto, M., Ene-Iordache, B. & Remuzzi, A. Transitional Flow in the Venous Side of Patient-Specific Arteriovenous Fistulae for Hemodialysis. *Ann Biomed Eng* **44**, (2016).

33. Colombo, M. *et al.* Superficial femoral artery stenting: Impact of stent design and overlapping on the local hemodynamics. *Comput Biol Med* **143**, (2022).

34. Candreva, A. *et al.* Current and Future Applications of Computational Fluid Dynamics in Coronary Artery Disease. *Reviews in Cardiovascular Medicine* vol. 23 Preprint at https://doi.org/10.31083/j.rcm2311377 (2022).

35. Malek, A. M., Alper, S. L. & Izumo, S. Hemodynamic shear stress and its role in atherosclerosis. *J Am Med Assoc* (1999) doi:10.1001/jama.282.21.2035.

36. Nordgaard, H. *et al.* Impact of competitive flow on wall shear stress in coronary surgery: Computational fluid dynamics of a LIMA-LAD model. *Cardiovasc Res* **88**, (2010).

37. Dolan, J. M., Kolega, J. & Meng, H. High wall shear stress and spatial gradients in vascular pathology: A review. *Annals of Biomedical Engineering* vol. 41 Preprint at https://doi.org/10.1007/s10439-012-0695-0 (2013).

38. Kawaguchi, T. *et al.* Distinctive flow pattern of wall shear stress and oscillatory shear index: Similarity and dissimilarity in ruptured and unruptured cerebral aneurysm blebs. *J Neurosurg* (2012) doi:10.3171/2012.7.JNS111991.

39. Mazzi, V. *et al.* A Eulerian method to analyze wall shear stress fixed points and manifolds in cardiovascular flows. *Biomech Model Mechanobiol* **19**, (2020).

40. Candreva, A. *et al.* Risk of myocardial infarction based on endothelial shear stress analysis using coronary angiography. *Atherosclerosis* **342**, (2022).

41. Mazzi, V. *et al.* Early Atherosclerotic Changes in Coronary Arteries are Associated with Endothelium Shear Stress Contraction/Expansion Variability. *Ann Biomed Eng* **49**, (2021).

42. De Nisco, G. *et al.* Deciphering ascending thoracic aortic aneurysm hemodynamics in relation to biomechanical properties. *Med Eng Phys* **82**, (2020).

43. Morbiducci, U. *et al.* Wall Shear Stress Topological Skeleton Independently Predicts Long-Term Restenosis After Carotid Bifurcation Endarterectomy. *Ann Biomed Eng* **48**, (2020).

44. Mazzi, V. *et al.* Divergence of the normalized wall shear stress as an effective computational template of low-density lipoprotein polarization at the arterial blood-vessel wall interface. *Comput Methods Programs Biomed* **226**, (2022).

45. Chiastra, C. *et al.* Coronary Artery Stenting Affects Wall Shear Stress Topological Skeleton. *J Biomech Eng* **144**, (2022).

46. Paul Jaccard. The Distribution of the Flora in the Alpine Zone. *New Phytologist* **11**, (1912).

47. Kim, E. S. H. *et al.* Interpretation of peripheral arterial and venous Doppler waveforms: A consensus statement from the Society for Vascular Medicine and Society for Vascular Ultrasound. *Vascular Medicine (United Kingdom)* **25**, (2020).